J Mater Sci (2009) 44:6125–6134
DOI 10.1007/s10853-009-3847-3

Microstructure and mechanical properties of AlN films obtained by plasma enhanced chemical vapor deposition

Gustavo Sánchez · B. Abdallah · P. Tristant · C. Dublanche-Tixier · M. A. Djouadi · M. P. Besland · P. Y. Jouan · A. Bologna Alles

Received: 28 July 2009 / Accepted: 25 August 2009 / Published online: 10 September 2009
© Springer Science+Business Media, LLC 2009

Abstract AlN films were prepared with a microwave plasma enhanced chemical vapor deposition reactor working at different process temperatures in order to obtain polycrystalline ⟨0001⟩ oriented films for piezoelectric applications. The films developed were characterized in terms of microstructure, composition, and mechanical properties. Crystalline development and a single orientation were obtained at high temperatures, where at the same time an increase in mechanical intrinsic stresses was observed. Well crystallized ⟨0001⟩ films were obtained at temperature as low as 500 °C. Furthermore, the evolution of microstructure with thickness at higher temperatures showed a single ⟨0001⟩ orientation with progressive increase of the texture as the thickness increased. This fact was related with changes in the observed microstructure along the film *z*-axis, evaluated by high resolution transmission electronic microscopy and selected area electron diffraction. Although orientation dispersion of these films, evidenced by the rocking curves FWHM, remained relatively high (>9°), they can be regarded as promising for piezoelectric applications. Annealing tests conducted at relatively high temperatures with films deposited at low temperature indicated that thermal effects have only a major effect during the film growth for the temperature values employed.

G. Sánchez (✉) · P. Tristant · C. Dublanche-Tixier
SPCTS, UMR CNRS 6638, Faculté des Sciences et Techniques, Université de Limoges, 123 Avenue Albert Thomas, 87060 Limoges, France
e-mail: gsanchez@fing.edu.uy

G. Sánchez · A. Bologna Alles
Departamento de Ingeniería de Materiales, Facultad de Ingeniería, Universidad de la República, Julio Herrera y Reissig 565, 11300 Montevideo, Uruguay

B. Abdallah · M. A. Djouadi · M. P. Besland · P. Y. Jouan
Institut des Matériaux Jean Rouxel, IMN, UMR 6502, Université de Nantes, 2 rue de la Houssinière BP 32229, 44322 Nantes, France

B. Abdallah
Atomic Energy Commission Syrian (AECS), 6091 Damascus, Syrian Arab Republic

Introduction

Aluminum nitride (AlN) is one of the most interesting piezoelectric materials in the fabrication of acoustic wave devices due to its high acoustic velocity and fairly large piezoelectric coupling coefficient. Single crystal films would be the ideal choice for these applications; however, high quality polycrystalline preferentially oriented films can be used with good success [1]. ⟨0001⟩ and ⟨10$\bar{1}$0⟩ oriented AlN films have been shown of interest for different piezoelectric applications [2].

The full width at half maximum (FWHM) observed in an X-ray diffraction (XRD) rocking curves has been used to evaluate AlN films orientation grade or texture. This parameter has been correlated with the piezoelectric performance for ⟨0001⟩ oriented AlN films, suggesting that a maximum dispersion value around a 4° is acceptable to obtain an adequate piezoelectric response [1]. Recent studies have shown that not only the FWHM of the rocking curve is important to define the piezoelectric performance, but also other characteristics of the microstructure of the films are determinant as well, such as the absence of "inversion domains" [3]. In this sense, it has been shown that 8° FWHM films could also result in optimal piezoelectric performance if the adequate microstructure is developed [3].

High quality AlN films have been grown by chemical vapor deposition (CVD) and molecular beam epitaxy (MBE) techniques using temperatures higher than 1000 °C and very low deposition rates [4]. Other techniques—such as reactive evaporation, pulsed laser deposition, and magnetron sputtering—have allowed to grow films at lower temperatures with good results. Particularly, the use of magnetron sputtering to produce these films at low temperatures has been investigated to a great extent [5]. Plasma enhanced CVD techniques (PECVD), in general, allow to reduce the process temperature due to the increase of the reactivity of the species in the reactor chamber by the plasma. Using a microwave PECVD reactor, polycrystalline AlN films were produced, as well as, their preferential orientation, either in the $\langle 0001 \rangle$ or $\langle 10\bar{1}0 \rangle$ directions was achieved [2].

It is well-known that the structure, crystallinity, texture, stress, and the piezoelectric properties of films deposited by plasma methods can change significantly as the film thickness increases [6–10]. Because of this, the object of this study was to optimize the deposition conditions of AlN thin films by microwave PECVD by observing the changes in the film characteristics with increasing thicknesses obtained at optimal deposition conditions, and relate this to the film growth mechanism in order to better understand the overall process.

Experimental details

Si (100) wafers of 20 × 20 mm were used as substrates for the deposition of AlN films. The wafers were ultrasonically cleaned in ethanol and acetone before placing them in the reactor chamber. A microwave PECVD reactor equipped with a substrate-holder capable of heating and/or to applying an RF-bias potential to the substrate was employed. AlN films were deposited by means of a nitrogen plasma in which tri-methyl-aluminum (TMA) was injected using argon as the carrier gas. The experimental conditions employed during AlN film depositions are shown in Table 1, where the substrate temperature was varied between 150 and 700 °C in this study.

XRD $\theta/2\theta$ patterns were recorded between 30 and 40° (2θ), with a scanning step of 0.05° (2θ), using a D-5000 diffractometer (Siemens Kristalloflex) equipped with Cu anode and a graphite back-monochromator. The incident angle (θ) was offset by 0.5° aiming to reduce the reflections of the Si (100) substrate. A measure of the average grain sizes of some films was estimated from the AlN (0002) reflection peaks taking the FWHM [11]. Rocking curves were obtained for the (0002) AlN reflection, and their FWHM were estimated to evaluate the orientation degree.

Table 1 Experimental conditions

Variable	AlN film growth
Microwave power (kW)	1.6
Nitrogen flow rate (sccm)	125
Argon flow rate (sccm)	50
TMA flow rate (sccm)	1
Chamber pressure (Pa)	1
Plasma–injector distance (cm)	3
Injector–substrate distance (cm)	4
RF bias potential (V)	No
Substrate temperature (°C)	150–700
Processing time (min)	0–15

sccm standard cubic centimeters per minute

Fourier transform infrared transmission spectroscopy (FTIR) spectra (Perking Elmer Spectrum One) were obtained in transmission mode between 4000 and 400 cm^{-1}, with 1 cm^{-1} step, at 300 K, using the spectrum of the Si substrate as background.

The composition of the films was elucidated by RBS (Rutherford backscattering spectrometry) to find the amount of aluminum in the film, as well as and nuclear reaction analysis (NRA) was employed to find the amounts of nitrogen, oxygen, and carbon present in the various samples. The analysis were carried out in an ultra-high vacuum chamber (base pressure: 2 × 10^{-6} Torr) and the beams were generated by an electrostatic Van de Graaf accelerator. While 2.0 MeV He^{+} were used for RBS analysis, 1.8 MeV d^{+} for N and O detection and 1.020 MeV d^{+} for C detection were used for NRA analysis.

The residual stresses in the films were deduced from the substrate curvature before and after film deposition according to Stoney's formula [12]:

$$\sigma_{\text{res}} = \frac{E_s e_s^2}{6(1 - v_s)} \frac{1}{e} \left(\frac{1}{R(e)} - \frac{1}{R_0} \right) \quad (1)$$

where R_0 is the radius of curvature of the bare Si substrate, $R(e)$ is the radius of curvature after the deposition of the film on the substrate, E_s and v_s are, respectively, the Young's modulus and Poisson ratio of the substrate, e_s and e are the thicknesses of the substrate and the film, respectively. The curvature of the substrate as well as the thicknesses of the films were evaluated with a profilometer, where the latter were also obtained from film cross-section micrographs obtained by scanning electron microscopy (SEM) (JEOL JSM 6400F).

Film thermal stresses were estimated according to [13]:

$$\sigma_{\text{the}} = \frac{E_f}{(1 - v_f)} (\alpha_f - \alpha_s)(T_d - T_a) \quad (2)$$

where the thermal expansion coefficients of the film and the substrate, respectively, were taken to be $\alpha_f = 4.1 \times 10^{-6}$ K^{-1}

[14] and $\alpha_s = 2.6 \times 10^{-6}$ K^{-1} [15], T_d and T_a the deposition and ambient temperatures, E_f and ν_f the film Young's modulus and Poisson's ratio.

Nanoindentation was performed on the films using a Nano Indenter XP™ (MTS Nano Instruments) with a Berkovich tip in order to determine the Young's modulus. This property was evaluated using the Oliver and Pharr's analysis technique [16]. The indentations were made in the continuous stiffness mode using a constant nominal strain rate of 0.05 s^{-1}, a frequency of 45 Hz, and a harmonic displacement of 2 nm.

The intrinsic stresses of the films were deduced using the above calculated stresses as:

$$\sigma_{int} = \sigma_{res} - \sigma_{the} \quad (3)$$

Surface morphology of the films was analyzed by atomic force microscopy (AFM) with the microscope (Molecular Imaging Scanner) operating in tapping mode near 75 kHz under ambient conditions. Silicon tips with a force constant of 2.8 N/m and a nominal radius of curvature of 20 nm were employed. The S_a roughness coefficient (arithmetic mean of the absolute value of the surface rugosity) was determined.

A fine structural study of the films was carried out by high resolution transmission electron microscopy (HRTEM) using a Hitachi HF 2000, and selected area electron diffraction (SAED) patterns were obtained with an acceleration voltage of 200 kV. Thin foils for transmission electron microscopy were prepared by mechanical polishing in a tripod polisher (30–0.025 μm) and thinned down to electron transparency using an ion milling technique.

Optical emission spectra of the plasma were recorded with a Jobin–Yvon THR1000 monochromator (ISA Division Instruments S.A.) which was coupled to the reactor chamber by an optical fiber. Photon detection was performed with a nitrogen cooled CCD (charge-coupled device) detector. The spectral resolution was better than 0.5 nm (FWHM).

The piezoelectric performance of selected films was characterized by piezoelectric force microscopy (PFM) technique, operating in contact mode, at a frequency of 10 kHz, by scanning 5 μm at a scan rate of 1 Hz during 3 s, and voltages between 0 and 10 V. The unclamped value of the piezoelectric coefficient (d_{33}) was estimated [1, 17].

Results and discussion

Process temperature

AlN films, 0.25 μm thick, were deposited on Si (100) in the aforementioned conditions (see Table 1), for substrate temperatures ranging from 150 to 700 °C. Figure 1 shows the XRD patterns obtained at different process temperatures. While the film obtained at 150 °C showed no significant crystalline development with the absence of AlN reflection peaks, the film obtained at 300 °C exhibited incipient reflection peaks for the different diffraction planes, indicating the beginning of a crystalline development with the use of increasing of substrate temperatures. For deposition temperature values of 500 and 700 °C, the intensity of the (0002) reflection peak began to exhibit a marked increase corresponding to the development of a ⟨0001⟩ orientation.

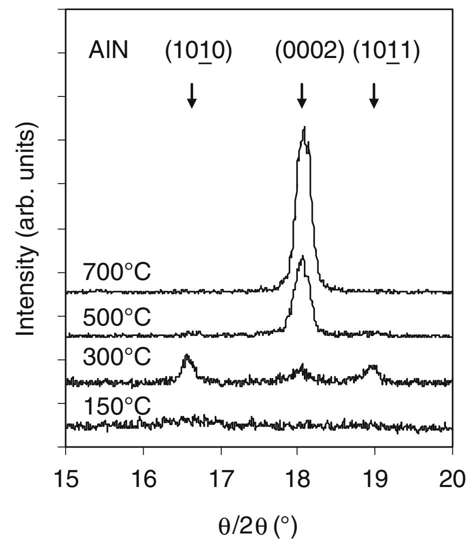

Fig. 1 XRD patterns at different temperatures for 0.25 μm thick films obtained on Si (100) substrate at 1 Pa, plasma–injector distance of 3 cm, injector–substrate distance of 4 cm, and no RF bias

Figure 2 shows the FTIR spectra for the films obtained at different temperatures. Al–N bands corresponding to E1(TO) and A1(TO) vibration modes were present in all cases (see Fig. 2a) [18], however, significant differences in shape in the convoluted peak were observed. The deconvolution of the latter using a Gaussian–Lorentzian fitting, pointed out to an increasing contribution of the E1(TO) band with higher process temperature, accompanied by a decrease of the A1(TO) band. Considering that the vibration modes E1(TO) and A1(TO) correspond, respectively, to the modes excited by a perpendicular and a parallel electric field to the *c*-axis of the AlN crystal, the relative increase of the E1(TO) mode can be associated with the development of a ⟨0001⟩ oriented film [18].

Simultaneously with these changes, a marked decrease of the impurity band located at around 2150 cm^{-1} (see Fig. 2b) was observed when higher substrate temperatures are employed. This band, traditionally assigned to a number of species, i.e., Al–C≡N, Al–H or Al–N_2 [2], are

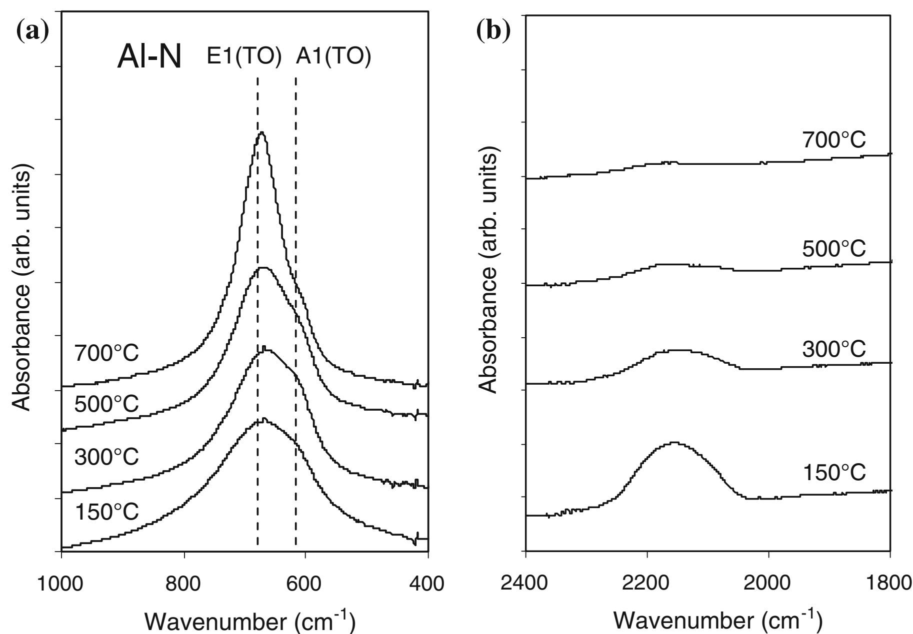

Fig. 2 FTIR spectra for AlN 0.25 μm thick films obtained on Si (100) substrate at 1 Pa, plasma–injector distance of 3 cm, injector–substrate distance of 4 cm, and no RF bias. Temperatures are indicated

typically present in PECVD AlN films, where the latter could be related with by-products derived from the aluminum precursor employed (TMA). OES spectra of the plasma during the deposition process (see Fig. 3) evidenced the presence of C–N species in the reactor chamber, which might result from the reaction between the nitrogen and precursor species that, in turn, can be incorporated in the film structure during its growth [19]. It is possible to speculate that, at low process temperatures, the impurities associated to the decomposition of TMA are incorporated in the film because of generally poor desorption conditions to become entrapped in the structure of the growing film.

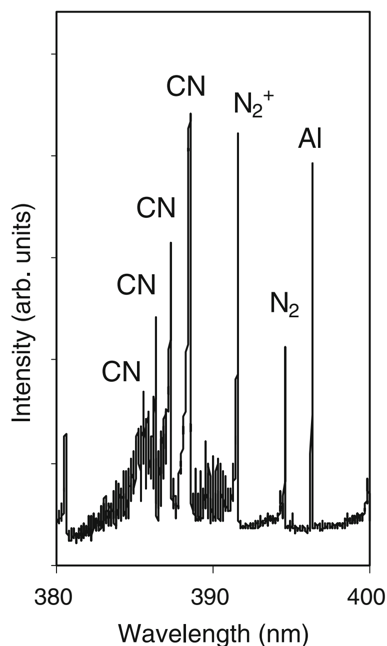

Fig. 3 Optical emission spectrum of the region between the injector and the substrate during the AlN deposition

The relatively low surface diffusion of AlN species did not allow a good crystal growth as well when the substrate temperature is markedly low. At higher temperatures, surface diffusion during the film growth allowed for a sizable crystalline development, and the evolution to a single ⟨0001⟩ orientation at higher temperatures is likely favored by the minimization of surface energy due to the fact that the plane parallel to the substrate surface has the highest packing fraction [20, 21].

Due to the difference between the thermal expansion coefficients of the substrate and the films, thermal stresses of different values were generated for each deposition temperature. These values were estimated using measured Young's modulus for each film, and +0.04, +0.10, +0.20, and +0.29 GPa were obtained for films deposited at 150, 300, 500, and 700 °C, respectively, where the positive sign indicates tension. By subtracting these values from the measured total residual stresses, increasing tensile intrinsic stresses for the different deposition temperatures resulted (see Fig. 4).

The grain boundary relaxation model [13] has been frequently used in the literature to explain the development of tensile intrinsic stresses in polycrystalline or amorphous films that exhibit columnar or fibrous microstructures. The interatomic attractive forces, acting across grain boundaries or gaps between grains and intercolumnar spaces on one hand, and the intragrain or intracolumn tensile forces imposed by the constraint caused by the adhesion of the film to the substrate on the other hand, are taken in account

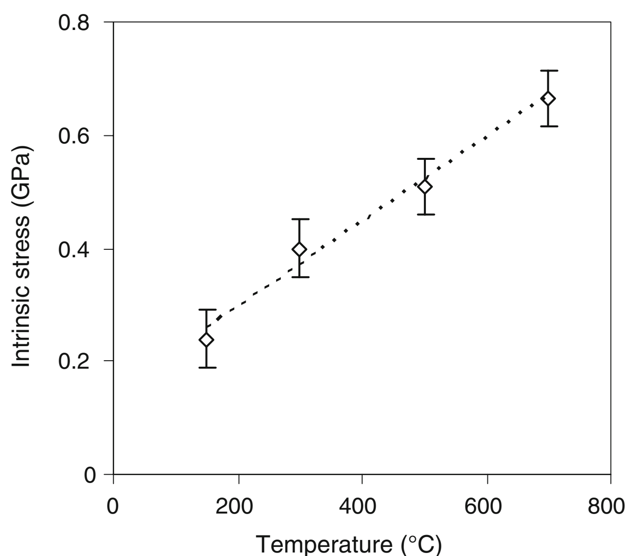

Fig. 4 Intrinsic stresses versus temperature for AlN films obtained on Si (100) substrate at 1 Pa, plasma–injector distance of 3 cm, injector–substrate distance of 4 cm, and no RF bias. Thicknesses: 0.25 μm

in this model. As a result, the induced stress is tensile since the film attempts to constrain itself. Therefore, for a given material, the development of increasing film tensile stress values could be related with higher film crystalline development. As observed, the change from a relatively amorphous and porous structure, obtained at low process temperatures, to columnar and well crystallized structures obtained at high process temperatures resulted in increasing tensile intrinsic stresses.

In addition to the above, the change in the thermal expansion coefficient of the AlN film of different crystallinity can be considered to introduce an extra unaccounted factor in the estimation of the film true intrinsic stress. Usually, an average reference value for the thermal expansion coefficient is taken into account when calculating thermal stresses, although strictly speaking in the case of AlN crystals with a hexagonal wurtzite type structure, two values of the linear thermal expansion coefficient are present, i.e., parallel and perpendicular to the *c*-axis. The thermal expansion anisotropy for AlN crystals has been quantified, and a ratio of $(\alpha_{perp}/\alpha_{par}) = 1.17 \pm 0.05$ over a wide temperature range was recorded [22], where the linear expansion coefficient along the *c*-axis is smaller than the perpendicular one. For films obtained at higher process temperatures—those that are well crystallized in the $\langle 0001 \rangle$ direction, i.e., with the *c*-axis perpendicular to the surface—it is likely that an underestimated value for the true thermal stress is calculated when compared to a non textured film, since thermal stresses generated in the film are mainly parallel to the substrate surface and therefore perpendicular to the *c*-axis. In turn, this leads to overestimating the true intrinsic stress value present in the film, something that it is likely to have happened in the past.

Annealing

In order to get a better understanding of the temperature effects onto the intrinsic stress and structure of a film deposited at low temperature, an AlN film obtained at 300 °C was annealed at 700 °C during 2 h in vacuum. The comparison of the XRD patterns (see Fig. 5) showed that no significant crystallization took place in the film due to the post-treatment. The difference in crystalline development and texture of the latter with films grown at 700 °C (see Fig. 5) suggests that thermal effects are relevant only during film growth. It can be speculated that higher temperature values during film growth allow for the surface diffusion of the incident species, as well as, promoting the desorption of impurities enhancing a better crystalline development.

The minimization of surface free energy favors the $\langle 0001 \rangle$ crystal orientation, however, once the film has been grown at low temperature (300 °C), it is not possible to obtain the same crystallization degree by annealing at higher temperatures (700 °C), probably because of the markedly slow rearrangement of the species involved considering the relatively high temperatures at which AlN undergoes sintering and ultimately melting.

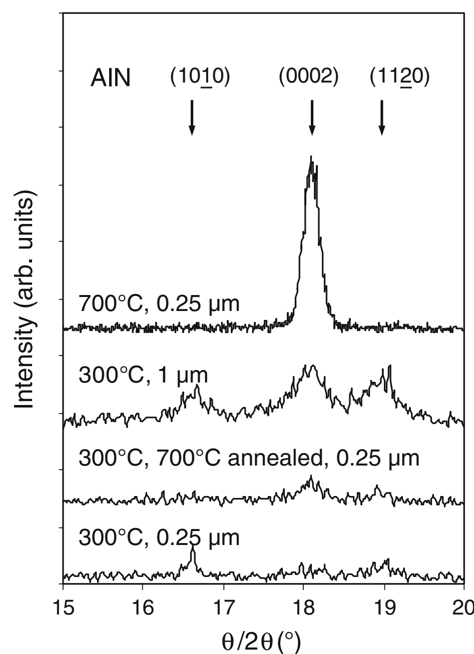

Fig. 5 XRD patterns for AlN films obtained on Si (100) substrate at 1 Pa, plasma–injector distance of 3 cm, injector–substrate distance of 4 cm, and no RF bias. Deposition temperatures, thicknesses, and post-treatment conditions are indicated

A 1 µm thick film was deposited at low temperature of 300 °C. As it is shown in Fig. 5, no significant differences in crystalline development and orientation could be observed as the film thickness increased. Consequently, substrate temperature during the deposition process appears to be a key factor for obtaining well crystallized films with ⟨0001⟩ preferential orientation, therefore, the effect of increasing film thickness, after the temperature is optimized, was studied.

Film thickness

AlN films were deposited on Si (100) substrate at the specified conditions, with a substrate temperature of 700 °C, and varying the process time, thicknesses between 0.12 and 1.15 µm were produced.

The evolution of the XRD patterns with film thickness showed only one orientation from the onset of the film growth, i.e., ⟨0001⟩, as well as a progressive increase in the size of the (0002) reflection peak (see Fig. 6a). FWHM estimated values from the (0002) reflection peak did not indicate that significant differences in average grain sizes developed as the film grew thicker.

Rocking curves obtained for the (0002) reflection for the different cases showed a progressive FWHM reduction with increasing film thickness, from 15 to 9° (see Fig. 6b), which is an indication of increasing ⟨0001⟩ texturing.

The FTIR transmission spectra of the films with different thicknesses exhibited the typical shape of AlN bands observed in Fig. 2 for 700 °C, with a progressive change in size with thickness as expected, however, no significant differences were distinguished concerning the size ratio of the AlN E1(TO) and the A1(TO) vibration modes.

RBS/NRA analyses of the 50, 500, and 1000 nm thick films, respectively (see Table 2) pointed out that an important decrease in the impurity concentrations, i.e., oxygen and carbon, with increasing thickness mainly from 50 to 500 nm took place. Since the latter results correspond to average impurity concentrations in the film, the significant decrease of the oxygen content between 50 and 500 nm could also be associated to the spontaneous oxidation of the AlN film surfaces when exposed to air [23, 24]. Similarly, the decrease of the film carbon content could also be associated mainly with the presence of impurities on the film surface resulting from the adsorption of ambient carbon containing gases or from the chamber environment from the TMA (precursor) after the deposition process. Although this, an improvement in the overall crystallization of the film could not be ruled completely out as a key factor in reducing the film average impurities levels.

Table 2 RBS/NRA analysis of the films with different thicknesses obtained on Si (100) substrate at 700 °C, 1 Pa, plasma–injector distance of 3 cm, injector–substrate distance of 4 cm, and no RF bias

Film thickness (µm)	Al (at.%)	N (at.%)	O (at.%)	C (at.%)
0.05	43.0 ± 2	46.2 ± 2	6.5 ± 0.3	4.3 ± 0.2
0.5	48.6 ± 2	45.9 ± 2	4.2 ± 0.2	1.3 ± 0.1
1.0	46.8 ± 2	48.2 ± 2	4.4 ± 0.2	0.6 ± 0.03

AFM images of the films showed that no basic differences in the shape of the surface topography could be observed, and regardless of the thickness of the film, the presence of tops associated with a film columnar microstructure was invariably recorded. However, an increase in size of the tops with increasing thickness was observed indicating that columns grew larger as the thickness of the film increased (see Fig. 7). The latter was accompanied, as expected, by an increase in the roughness of the films (from $S_a = 0.9$ nm at 1.5 min to 7.6 nm at 9 min). This fact

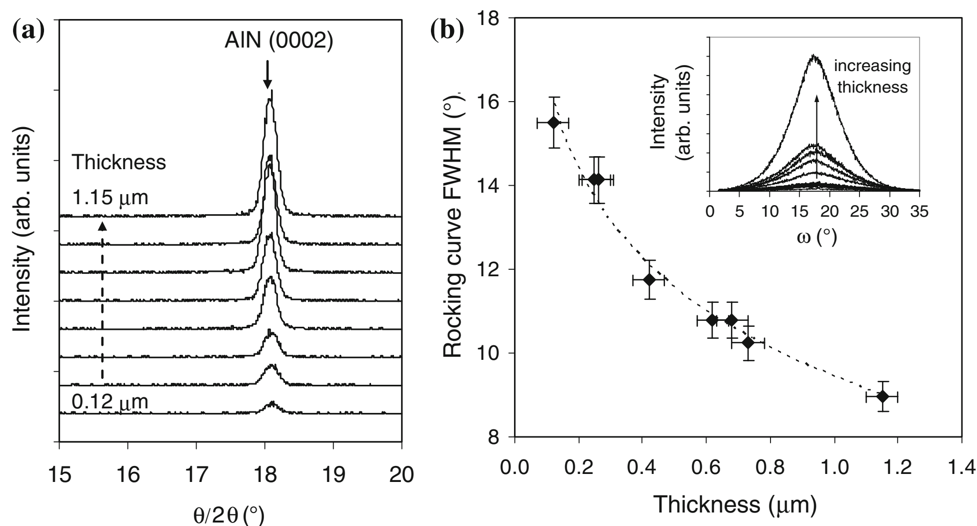

Fig. 6 Evolution XRD patterns (**a**) and rocking curve FWHM (**b**) with thickness for AlN films obtained on Si (100) substrate at 700 °C, 1 Pa, plasma–injector distance of 3 cm, injector–substrate distance of 4 cm and no RF bias

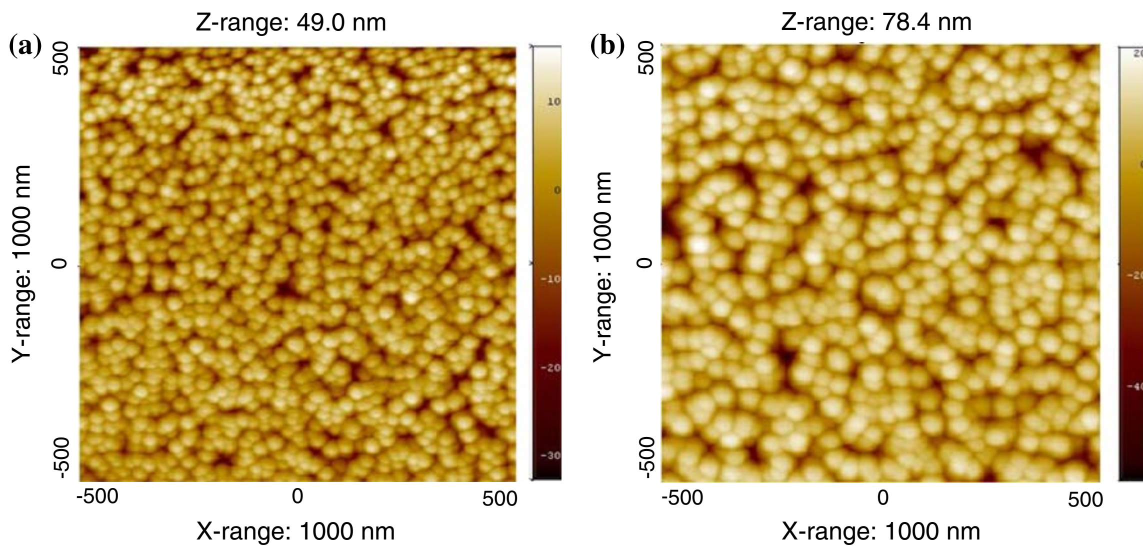

Fig. 7 AFM images of the AlN film surfaces obtained on Si (100) substrate at 700 °C, 1 Pa, plasma–injector distance of 3 cm, injector–substrate distance of 4 cm, and no RF bias. Process time and measure roughness: **a** 4.5 min, $S_a = 4.8$ nm, **b** 9 min, $S_a = 7.8$ nm

suggests that for higher thicknesses, a better crystalline development is obtained at the surface, with the columns top formed by larger grains. At the same time and as it was previously shown, this was accompanied by an improvement in the overall film preferential orientation.

Residual stresses were measured for all thicknesses between 0.12 and 1.25 μm. Since the films were obtained at 700 °C, thermal stresses of +0.29 GPa were estimated by using Eq. 2. Thus, intrinsic stresses were deduced for the different film thicknesses (see Fig. 8) where tensile intrinsic stresses were obtain in all the cases. Increasing stresses were calculated up to a maximum value at around

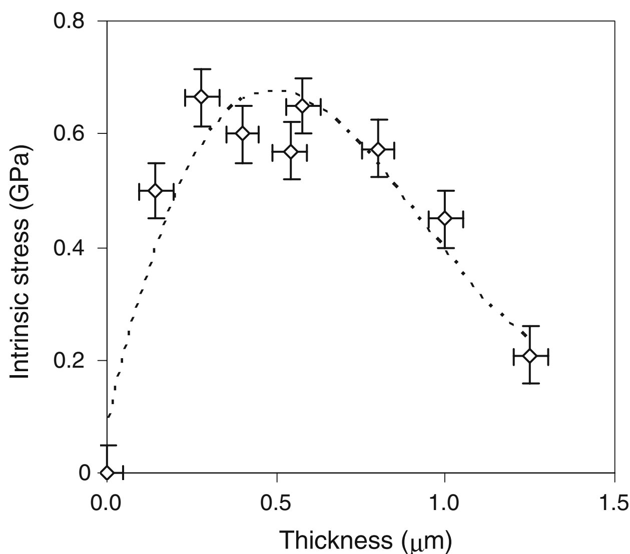

Fig. 8 Intrinsic stresses versus thickness for AlN films obtained on Si (100) substrate at 1 Pa, 800 °C, plasma–injector distance of 3 cm, injector–substrate distance of 4 cm, and no RF bias

0.25 μm, followed by gradual decrease as the films grew thicker. The above evolution of tensile residual stresses with increasing thickness in thin films has been recorded in the past, and several models [13, 25, 26] had been put forward to explain this behavior.

A film cross-section of a ⟨0001⟩ oriented AlN film deposited at 700 °C, on Si (100) substrate, 1 μm thickness, was analyzed using HR TEM and SAED. The TEM cross-section image of the film (see Fig. 9a) showed a columnar structure. SAED patterns were taken over 400 nm diameter circular areas along the film *z*-direction. The first pattern (see Fig. 9b) was located at the substrate giving the typical pattern of Si single crystal. The second pattern corresponds to the lower portion of the AlN film showing two intense arcs corresponding to (0002) reflections associated with (0001) planes with a misalignment angle of 15°. The third pattern (see Fig. 9c), corresponding to about the center of the film, exhibited an increasingly ⟨0001⟩ textured columnar film with a misalignment angle of 6°. Finally, the pattern obtained at the surface of the film showed a diffraction pattern that approaches that of a ⟨0001⟩ oriented AlN single crystal [27]. Consequently, although only the ⟨0001⟩ orientation was present from the film–substrate interface up to the film surface, the texture as well as the crystalline quality markedly improved as the film grew thicker.

In order to better understand the deposition process of the film grew thicker, high resolution TEM images of the film growth direction (*z*-direction) were obtained. The AlN/Si interface showed a 4 nm thick amorphous layer (see Fig. 10a), followed by a polycrystalline AlN layer exhibiting crystallites mostly ⟨0001⟩ oriented and few $\langle 10\bar{1}1\rangle$ oriented. The images of the film at the middle and near the

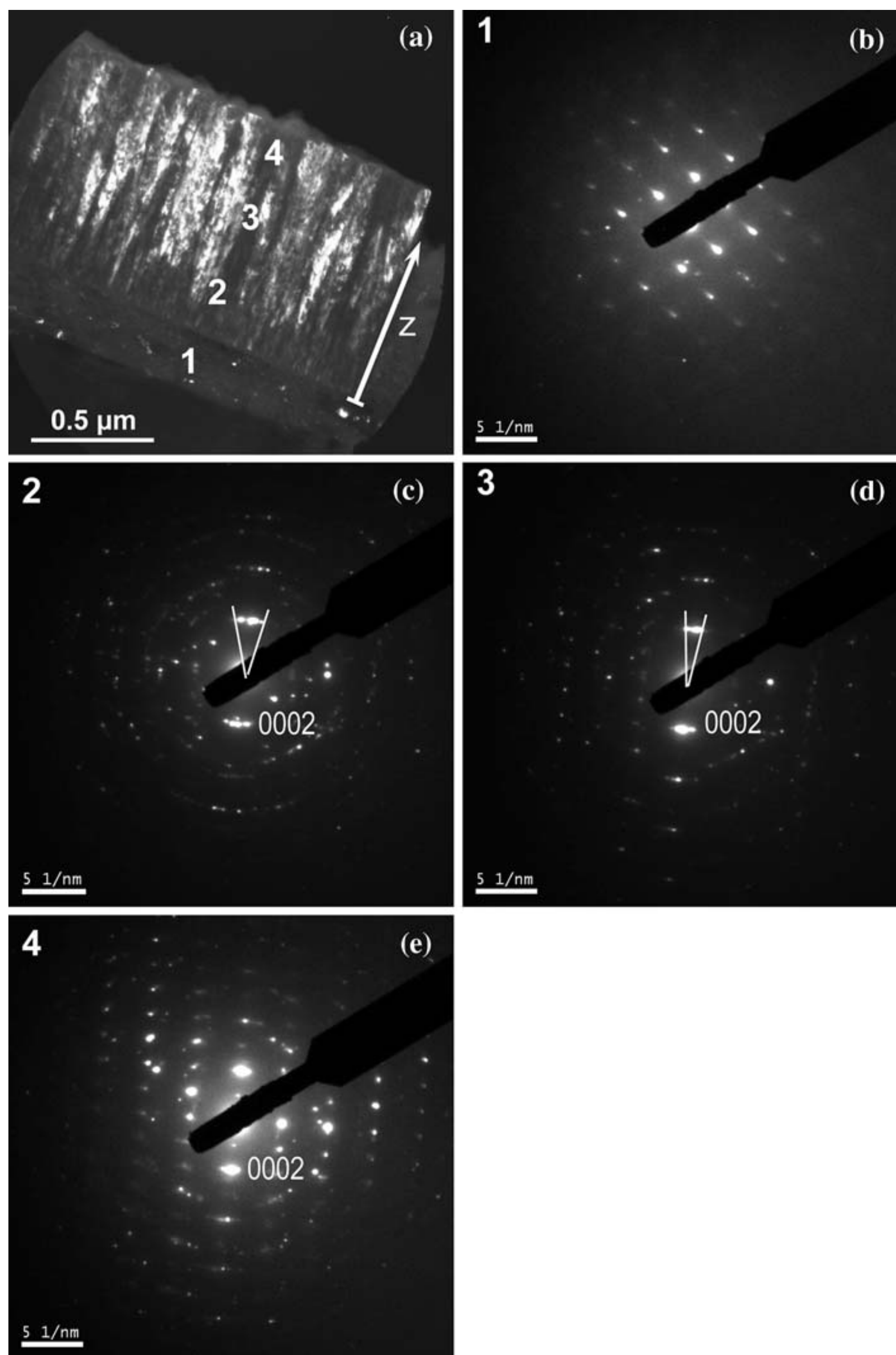

Fig. 9 TEM image and evolution in the film *z*-direction of selected area electron diffraction patterns for one AlN film obtained on Si (100) substrate at 700 °C, 1 Pa, plasma–injector distance of 3 cm, injector–substrate distance of 4 cm, and no RF bias; thickness: 1 µm: **a** film pattern locations, **b** electron diffraction pattern of the substrate, **c**, **d**, **e** electron diffraction patterns of the AlN film at the bottom, middle and top of the profile, with zone axis [01$\bar{1}$0]

film surface (Fig. 10b) showed a columnar structure with exclusively ⟨0001⟩ oriented crystallites with inter-reticular distances of about 0.250 nm. Average grain sizes around 45 nm were observed, where the latter value corresponded to about the top diameter of the columns (see Fig. 7b), in agreement with the size range estimated by XRD and AFM measurements.

All the previous observations are consistent with the fact that an improvement of the crystalline quality and texture takes place as the film thickness increases. According to HRTEM evidence as well as previous results [2], no significant epitaxial effects between the growing film and the substrate were observed that could favor a particular texture development from the onset of film growth. Thus, the apparent dominant variable to control the crystallization as well as the orientation, once the total reactor chamber pressure is set [2], is the substrate temperature which allowed the growth of the ⟨0001⟩ oriented film that minimizes the excess free energy of the surface [20, 21]. Consequently, it is possible to speculate that at the onset of

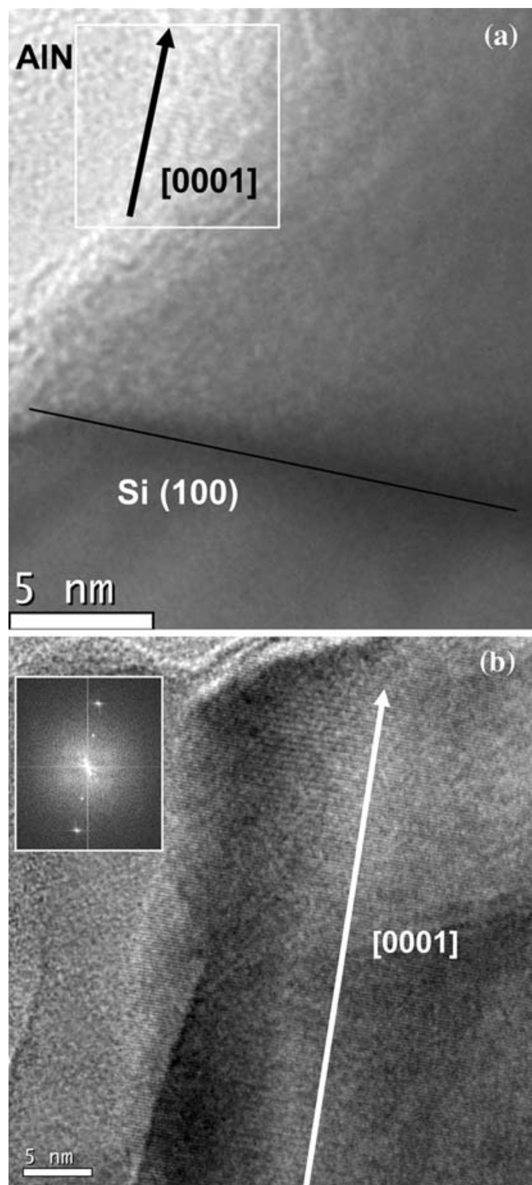

Fig. 10 HR TEM images in the growth direction (*z*-direction) of an AlN film obtained on Si (100) substrate at 700 °C, 1 Pa, plasma–injector distance of 3 cm, injector–substrate distance of 4 cm, and no RF bias; thickness 1 μm: **a** adjacent to the substrate, **b** near the top of the column, with the corresponding FFT pattern

film growth, an amorphous interlayer is developed onto which larger and better oriented crystallites develop as the film growths. Similar tendencies have been observed in films obtained by PVD techniques [6, 28].

Piezoelectric performance

A piezoelectric coefficient d_{33} of a ⟨0001⟩ oriented AlN film deposited at 700 °C, on Si (100) substrate, 1 μm thickness, was obtained by PFM in order to confirm that the obtained films were adequate for piezoelectric applications. A d_{33} value of 5.8 ± 1.2 pm/V was obtained in the range of the optimum values previously informed [1].

Conclusions

The substrate temperature during film growth was a key factor in the crystalline development of the deposited films. A change in the film microstructures with increasing temperature was observed, ranging from amorphous films obtained at 150 °C to well crystallized ⟨0001⟩ textured films observed at 700 °C.

Well crystallized films of increasing thickness obtained at 700 °C showed no change in the preferential crystalline orientation, i.e., ⟨0001⟩ for all the cases, but progressive texturing and crystalline quality improvement was observed by XRD rocking curves, TEM, SAED, as well as, in the morphology of the film surfaces observed by AFM. Contrary to this, it was observed that at relatively low temperatures, i.e., 300 °C, increasingly thicker films did not exhibit higher crystallinity nor texturing, thus, the improvement of film microstructure with thickness takes place only at higher temperatures.

No improvements in the microstructure were observed in films obtained at lower substrate temperatures by annealing them at the higher temperatures used in this study. This indicates that this variable is of marked significance only during film growth, suggesting that surface diffusion during this stage controls the process allowing for the rearrangement of the arriving species to crystallize properly. At the same time, higher substrate temperatures may promote the desorption of impurities derived from by-products present in the reaction chamber, e.g., C–N species.

The analysis of the microstructure in *z*-direction of a 1 μm thick film by HRTEM showed a marked improvement in the film crystalline quality and texture from the substrate interface to the film surface. The latter plus the aforementioned facts suggest that the microstructure of the film is mainly defined during the deposition of each and every layer and not by a bulk secondary recrystallization process, where epitaxial effects from the underlying layer could play a role in improving texturing as the film grows.

It was observed that a progressive increase in the film estimated tensile intrinsic stress resulted with increasing process temperature. This was related to the change in the film morphology, as well as, to the anisotropy of the thermal expansion coefficient, where the development of the ⟨0001⟩ preferential orientation could also possibly contribute to a calculated intrinsic stress increase by underestimating the true value of the thermal stress build up.

Intrinsic stresses showed the typical evolution with thickness found in the past in thin films deposited from the

vapor phase. This is consistent with the evolution of the film microstructure obtained by an initial coalescence of clusters followed by an ulterior column growth with shadowing effects.

Thicker AlN films obtained at higher temperatures, due to their microstructure and FWHM rocking curve values, exhibited an incipient but promising piezoelectric performance.

Acknowledgements The authors wish to acknowledge Eric Gautron for the HRTEM and SAED analysis made at the Institute des Materiaux Jean Rouxel, Université de Nantes, and to Valérie Coudert for AFM images obtained at the SPCTS laboratory, Université de Limoges.

References

1. Tonisch K, Cimalla V, Foerster Ch, Romanus H, Ambacher O, Dontsov D (2006) Sens Actuators A 132:658
2. Sánchez G, Wu A, Tristant P, Tixier C, Soulestin B, Desmaison J, Bologna Alles A (2008) Thin Solid Films 516:4868
3. Sanz-Hervás A, Clement M, Iborra E, Vergara L, Olivares J, Sangrador J (2006) Appl Phys Lett 88:161915
4. Semond F, Cordier Y, Grandjean N, Natali F, Damilano B, Vézian S, Massies J (2001) Phys Status Solidi A 188:501
5. Chen CS, Hwang BH, Lu HY, Hsu TC (2002) J Phys D Appl Phys 35:2608
6. Nouveau C, Djouadi MA, Banakh O, Sanjines R, Levy F (2001) Thin Solid Films 398:490
7. Ben el Mekki M, Djouadi MA, Guiot E, Mortet V, Pascallon J, Stambouli V, Bouchier D, Mestres N, Nouet G (1999) Surf Coat Technol 116–119:93
8. Meng WJ, Sell JA, Eesley GL, Perry TA (1993) J Appl Phys 74:2411
9. Abdallah B, Chala A, Jouan P-Y, Besland MP, Djouadi MA (2007) Thin Solid Films 515:7105
10. Hwang BH, Chen CS, Lu HY, Hsu TC (2002) Mater Sci Eng A 325:380
11. de Keijser Th, Mittemeijer E, Rozendaal H (1983) J Appl Crystallogr 16:309
12. Stoney GG (1909) Proc R Soc London A 82:172
13. Pauleau Y (2002) In: Nalwa HS (ed) Handbook of thin film materials, vol 1. Academic Press, New York
14. Chakrabarti K, Chattopadhyay KK, Chauhuri S, Pal AK (1997) Mater Chem Phys 50:50
15. Kawamoto N, Fujita M, Tatsumi T, Horikoshi Y (2003) Jpn J Appl Phys 42:7209
16. Oliver WC, Pharr GM (1992) Mater Res Soc Symp Proc 7:1564
17. Lefki K, Dormans G (1994) J Appl Phys 76:1764–1767
18. Sanz-Hervás A, Iborra E, Clement M, Sangrador J, Aguilar M (2003) Diamond Relat Mater 12:1186
19. Meikle S, Nomura H, Nakanishi Y, Hatanaka Y (1990) J Appl Phys 67:483
20. Lee JW, Cuomo JJ (2005) J Am Ceram Soc 88(7):1977
21. Mahieu S, Ghekiere P, Depla D, De Gryse R (2006) Thin Solid Films 515:1229
22. Slack GA, Bartram SF (1975) J Appl Phys 46:89
23. Jokinen J, Haussalo P, Keinonen J, Ritala M, Riihela D, Leskepi M (1996) Thin Solid Films 289:159
24. Mahmood A, Rakov N, Xiao M (2003) Mater Lett 57:1925
25. Doerner MF, Nix WD (1988) Crit Rev Solid State Mater Sci 14:225
26. Nix WD, Clemens BM (1999) J Mater Res 14:3467
27. Lebedev V, Jinschek J, Kraüsslich J, Kaiser U, Schröter B, Richter W (2001) J Crystal Growth 230:426
28. Martin F, Muralt P (2004) J Vac Sci Technol A 22:361